molecular pharmaceutics

pubs.acs.org/molecularpharmaceutics Article

Exploring the Toxicity, Lung Distribution, and Cellular Uptake of Rifampicin and Ascorbic Acid-Loaded Alginate Nanoparticles as Therapeutic Treatment of Lung Intracellular Infections

Ivana R. Scolari, Ximena Volpini, María L. Fanani, Benjamín De La Cruz-Thea, Lautaro Natali, Melina M. Musri,* and Gladys E. Granero*

Cite This: *Mol. Pharmaceutics* 2021, 18, 807−821 Read Online

ABSTRACT: Nanotechnology is a very promising technological tool to combat health problems associated with the loss of effectiveness of currently used antibiotics. Previously, we developed a formulation consisting of a chitosan and tween 80-decorated alginate nanocarrier that encapsulates rifampicin and the antioxidant ascorbic acid (RIF/ASC), intended for the treatment of respiratory intracellular infections. Here, we investigated the effects of RIF/ASC-loaded NPs on the respiratory mucus and the pulmonary surfactant. In addition, we evaluated their cytotoxicity for lung cells *in vitro*, and their biodistribution on rat lungs *in vivo* after their intratracheal administration. Findings herein demonstrated that RIF/ASC-loaded NPs display a favorable lung biocompatibility profile and a uniform distribution throughout lung lobules. RIF/ASC-loaded NPs were mainly uptaken by lung macrophages, their primary target. In summary, findings show that our novel designed RIF/ASC NPs could be a suitable system for antibiotic lung administration with promising perspectives for the treatment of pulmonary intracellular infections.

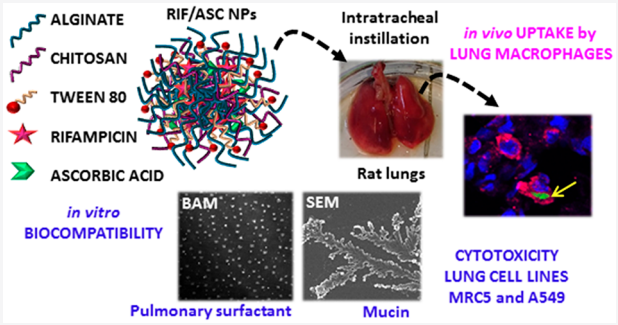

KEYWORDS: *rifampicin, ascorbic acid, nanoparticles, intratracheal administration, cytotoxicity, respiratory barriers*

1. INTRODUCTION

Infections caused by intracellular bacteria in the lower respiratory tract are one of the leading causes of death worldwide, mainly in developing countries.[1−4] In particular, pulmonary intracellular infections are difficult to eradicate due to various contributing factors. Among them, the lung's microenvironment constitutes a niche in which the bacteria are protected against the host's humoral response as well as from antibiotic therapy. Such protection can lead to the emergence of antibiotic resistance[5] in addition to the lack of new effective antibiotics against microorganisms.[6−8] Treatments currently used for lung infections produced by intracellular bacteria mainly consist of oral or intravenous (IV) administration of high doses of antibiotics by increasing the risks of side effects and toxicity.[9] In contrast, a targeted pulmonary antibiotic delivery for the treatment of respiratory infections has the benefit of achieving higher local antibiotic concentrations with minimal systemic exposure to the drug, hence, minimizing side effects and enhancing antibiotic action.[10−14]

However, factors related to biopharmaceutical characteristics of antibiotics including a poor intracellular penetration into mammalian cells like phagocytic alveolar macrophages (AMs), particle properties like size, shape, surface chemistry, and hygroscopicity, and physiological barriers on the respiratory tract such as the mucociliary clearance and the pulmonary surfactant (PS) are obstacles for effective deposition and retention of inhaled nanoparticle formulations in deep lung areas.[15−20]

To overcome all of these limitations, nanomaterials are the most promising strategy as potential antibiotic carriers. In particular, nanoparticles (NPs) based on natural glycopolymers have been explored for targeting antibiotics to specific pulmonary tissues and cells.[21−23] Among the advantages of these systems are their ability to link to several carbohydrate receptors present in mammalian cells as well as in bacteria due to their versatile physicochemical properties and biocompatibility.[24−27]

In previous studies, we documented the significant biocide activity of our engineered antibiotic rifampicin (RIF) and antioxidant ascorbic acid (ASC) coloaded into alginate (ALG)

Received: June 30, 2020
Revised: December 11, 2020
Accepted: December 14, 2020
Published: December 24, 2020

https://dx.doi.org/10.1021/acs.molpharmaceut.0c00692
Mol. Pharmaceutics 2021, 18, 807−821

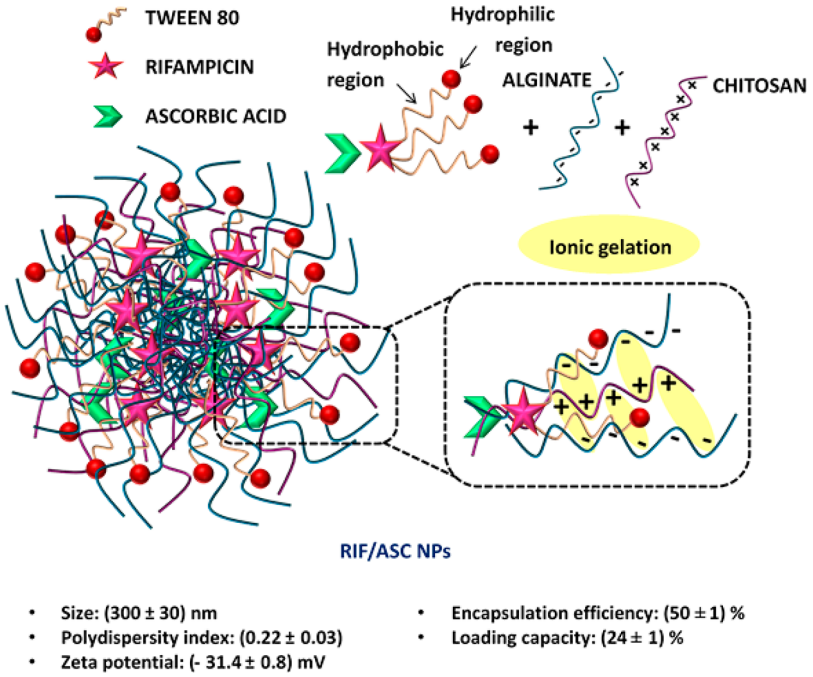

Figure 1. General schematic description and main characteristics of RIF/ASC NPs.

nanoparticles (NPs) functionalized by surface coating with the natural glycopolymer chitosan (CS) and the neutral surfactant tween 80 (T80) against different *Mycobacterium tuberculosis*, methicillin-sensitive *Staphylococcus aureus* (MSSA), and methicillin-resistant *Staphylococcus aureus* (MRSA) strains.[28,29] The proposed mechanism of action for this novel nanocarrier might be based on the antibiotics' effects and the NPs' surface features. These characteristics have an essential role in the NPs' adhesion on the bacterial surface and the induction of alterations in the bacterial cell membrane integrity and in the RIF cell uptake into bacteria.

In this study, we aim to acquire a comprehensive understanding of the potential use of our recently developed RIF/ASC-loaded NPs as a strategy for targeting them to the deeper lung areas and, therefore, as a promising therapy for respiratory intracellular infections. To this purpose, it is mandatory to explore key factors related to the effectiveness of this formulation for treating alveolar intracellular infections after inhaled administration. Consequently, in this work, we attempted to study the RIF/ASC-loaded NP interactions with important lung barriers, their potential lung cell toxicity, and lung distribution.

One of the first barriers that the formulations targeting the lower airways have to overcome is the PS. This is the lining layer in the deep lungs, whose main function is to avoid the cohesion of the alveolar surface and the bronchiolar walls.[30,31] Therefore, it is essential to preserve the functionality of the lung surfactant after contacting NPs.[32] However, interactions between NPs with the surfactant layer determine the fate of the inhaled carriers and their potential effects. To address the impact of the RIF/ASC-loaded NPs on the lung surfactant biophysical function and *vice versa*, *in vitro* experiments using an exogenous pulmonary surfactant from bronchoalveolar lavage fluid of bovine lungs, PROSURF-B, were performed.

Another biological barrier that NPs must overcome to reach the deepest regions of the lungs is the pulmonary mucus that covers the lung epithelium. The mucus has the function of lubricating and protecting the lung tissue by efficiently trapping and removing bacteria and foreign particles through the mucociliary clearance mechanism of the lungs, also contributing to the maintenance of healthy hydration of the tissue. Therefore, the mucus limits the penetration of the NPs into target tissues as well.[33] The mucus is a viscoelastic biopolymer gel mostly constituted of gel-forming glycoproteins known as mucins, which also determine the typical viscoelastic behavior of mucus.[34] Mucin molecules are characterized by containing a central protein core with regions of O-linked glycosylation and nonglycosylated domains.[35,36] In order to elucidate if the RIF/ASC-loaded NPs would be adhesively trapped in airway mucus following their inhalation, *in vitro* studies were conducted using porcine gastric mucin (PGM) as a model. These experiments aim to understand the impact of RIF/ASC-loaded NPs on the mucin network structure after contact.

Antibiotics must penetrate the lung cells to attain the concentration necessary to exert an effective intracellular biocide killing. Indeed, suboptimal drug concentrations typically exhibit weak antimicrobial activity and additional concerns regarding antibiotic resistance.[37,38] On the basis of these considerations, the potential cytotoxic effects of the RIF/ASC-loaded NPs were evaluated in human alveolar epithelial (A549) and human lung fibroblast (MRC5) cell lines.

Finally, in order to explore the biodistribution of NPs in the target organ and the type of cells that could uptake them, we conducted *in vivo* experiments performing intratracheal delivery of NPs labeled with the isothiocyanate fluorophore, FITC (NPs-FITC), at different time points in rats, followed by flow cytometry. In these experiments, we also evaluated the spleen, which is known to participate in the clearance of immune cells.[39]

2. MATERIALS AND METHODS

2.1. Materials. Low viscosity sodium alginate (ALG, MW ~ 70 000−100 000 Da, viscosity: ~4−12 cP, 39% content of α-L-guluronate and 61% content of β-D-mannuronate), commer-

https://dx.doi.org/10.1021/acs.molpharmaceut.0c00692
Mol. Pharmaceutics 2021, 18, 807−821

cially available low molecular weight chitosan (MW ~ 50 000−190 000 Da and ~85% degree of deacetylation), and T80 were purchased from Sigma-Aldrich (Buenos Aires, Argentina). Calcium chloride (Lot 44575) and rifampicin (Lot 107012) were purchased from TodoDroga (Córdoba, Argentina) and were used without further purification. Pig Gastric Mucin (PGM) type III was purchased from Sigma-Aldrich (Buenos Aires, Argentina), product code M1778.

Water was purified with a Milli-Q Purification system (Millipore Bedford, USA). Chemicals were of reagent grade or higher.

2.2. Preparation of NPs. RIF/ASC-loaded NPs were obtained following our previous report.[28]

Briefly, an ionic gelation method was employed to prepare the empty NPs or RIF/ASC-loaded NPs (RIF/ASC NPs). A 0.05% w/v $CaCl_2$ aqueous solution was added as a cross-linking agent to an aqueous solution containing 0.06% w/v ALG (pH 5.5) and RIF/ASC solubilized in 1% w/v T80 aqueous solution, followed by the subsequent addition of 0.05% w/v CS in 1% v/v acetic acid aqueous solution (pH 4.5). Empty NPs were prepared following the previously described procedure with the difference that the 1% w/v T80 aqueous solution did not contain RIF/ASC. Lyophilized empty NPs or RIF/ASC NPs were obtained by freeze-drying empty NPs or RIF/ASC NPs pellets prepared by using a LabconcoFreezone 6 freeze-dry system. For this procedure, a 1% w/v sucrose aqueous solution was added as a cryoprotectant agent.

The encapsulation efficiency (%EE) and loading capacity (% LC) of RIF into NPs were determined indirectly by subtracting the free RIF remanent in the supernatant separated from unbound RIF by centrifugation at 32 000*g*, 15 min, 4 °C from the original amount of RIF used to obtain the NPs. Free RIF in the supernatant was quantified by UV−vis spectrometry (λ = 334 nm).

The %EE and %LC of RIF loaded into NPs were calculated as follows (eqs 1 and 2, respectively):

$$\%EE = \frac{\text{drug}_{\text{total}}\,(\text{mg}) - \text{drug}_{\text{supernatant}}\,(\text{mg})}{\text{drug}_{\text{total}}\,(\text{mg})} \times 100 \quad (1)$$

$$\%LC = \frac{\text{drug in NPs}\,(\text{mg})}{\text{drug NPs}\,(\text{mg})} \times 100 \quad (2)$$

A general schematic description of the experimental design, along with the main features of the NPs obtained, is displayed in Figure 1.

2.3. *In Vitro* Physicochemical Interactions between an Exogenous Pulmonary Surfactant Model and RIF/ASC NPs. In order to delineate potential adverse biophysical effects of the inhaled RIF/ASC-loaded NPs on the pulmonary health after their exposition to the PS, the nature of the biophysical interactions between the animal-derived natural PS, with either empty NPs or RIF/ASC-loaded NPs dispersions was determined. We investigated the morphological microstructure evolution of PROSURF-B as a function of the incubation time in saline solution at 37 °C by means of combined use of optical and scanning electron microscopy and dynamic light scattering (DLS).

Experiments were carried out using the commercially available bovine surfactant PROSURF-B (lot 0432), which was generously provided as a gift from Nialtec S.A. (Buenos Aires, Argentine). PROSURF-B is a bovine bronchoalveolar lavage extract in chloroform solution containing polar lipids (94−80% phospholipids, 4.40% cholesterol, and 0.80% of SP-B and SP-C hydrophobic proteins). The solid surfactant was obtained by evaporating the organic solvent and measured with a rotary evaporator (BÜCHI Rotavapor R-114, Mexico) at 25 °C. Subsequently, the PS in the solid state was suspended in 5 mL of a 0.85% w/v NaCl solution, under stirring at 50 °C for 3 h. Interactions between PS and empty NPs or RIF/ASC NPs were assessed by mixing 2 mL of the PS in 0.85% w/v NaCl solution (2.9% w/v), empty NPs, or RIF/ASC NPs. For this purpose, 40 mg of NPs powder was resuspended in 1 mL of phosphate-buffer saline (PBS). Incubation of the before-mentioned mixtures was performed for periods of 5 or 24 h, under stirring, at 37 °C. Subsequently, particle size and surface charge of the mixtures were determined by DLS and ζ potential measurements, respectively, using a DLS (ZetasizerNano ZS, Malvern, UK). All measurements were performed in triplicate at room temperature. The diameter and PDI of particle size of NPs were estimated using the CONTIN algorithm analysis through inverse Laplace Transformation of the autocorrelation function. For scanning electron microscopy (SEM), a double-sided tape was placed on suitable support for SEM, and a plate of polished silicon Micro Nano 10-008145 was added to it. Then, ~10 μL of the mixture between NPs and PS previously incubated for 24 h at 37 °C or the saline 0.85% w/v NaCl solution, used as a control, was transferred to the silicon slice, dried at 30 °C, and sputter-coated with gold to be imaged by SEM (SUPRA 40 (ZEISS)). For light microscopy (LM), aliquots of NPs-PS mixtures were placed on clean glass slides, which were covered with coverslips and imaged with an optical microscope (ZEISS, West Germany).

Interactions of the PS with empty and RIF/ASC-loaded NPs as well as T80 were investigated by analyzing the change in the surface tension of the buffer (PBS) and by studying their effect on PS (PROSURF-B) Langmuir films at the air−water interface. In addition, their impact on the lateral PS monolayer organization was evaluated using Brewster angle microscopy (BAM).

Surface tension (γ) experiments were performed by measuring γ of the bare surface of PBS with a Pt plate by the Wilhelmy method. The equipment used was a homemade circular Langmuir balance controlled by an electronic unit (Monofilmetter, Mayer, Gottingen). A decrease in γ was registered after injection into the subphase of a stock solution of empty NPs or RIF/ASC-loaded NPs (1 mg/mL) in order to reach a final concentration of 5, 50, 100, 200, and 400 μg/mL and incubation for 20 min. A similar study was performed by adding only T80 in a concentration equivalent to its content in NPs preparations.

PS monolayer visualization was performed by BAM. Langmuir films of PS were constructed by spreading 10 μL of a chloroformed solution of PS (1 mM) onto the surface of PBS (210 cm^2) placed in a KSV Minitrough equipment (KSV, Helsinski, Finland). The surface pressure (π) was calculated as $\pi = \gamma_{\text{buffer}} - \gamma_{\text{film}}$. The initial π was <1 mN/m. Film compression was performed at a speed of 6 cm^2/min (10 $Å^2$ $molec^{-1}$ min^{-1}) until reaching 10 mN/m. Empty or RIF/ASC-loaded NPs were added to reach a surface concentration of 130 $\mu g/cm^2$ and further compressed until collapse.[40] The film was simultaneously imaged with a BAM microscope (Nanofilm EP3sw imaging ellipsometer, Accurion GmbH, Gottingen, Germany setted in BAM mode) equipped with a 532 nm laser, a 10× objective, and a CCD camera operating at a resolution

https://dx.doi.org/10.1021/acs.molpharmaceut.0c00692
Mol. Pharmaceutics 2021, 18, 807−821

of 0.52 μm/px. A zero reflection was set with a polarized 532 λ laser incident on the bare aqueous saline solution at the experimentally calibrated Brewster angle ($\theta_B \sim 53.164°$). For better visualization, the image background was subtracted, and the gray level of the images was modified, selecting the range 0−160 from the original 0−255 scale. Temperature = 22 ± 1 °C.

2.4. Interactions between RIF/ASC NPs with Pig Gastric Mucin (PGM). In this study, a PGM hydrogel was used as a respiratory mucosal barrier model to evaluate biophysical interactions between mucin and empty NPs or RIF/ASC-loaded NPs in terms of investigating changes in the rheological properties and the microscopic gel structure of mucin exposed to the NPs. In addition, interactions of NPs with mucin were evaluated using DLS because this technique provides sensitive evidence of the mucin structure and aggregation state. PGM was chosen because it contains MUC5AC and MUC5B, found in many mucosal surfaces, including the respiratory tract. At neutral pH, the overall negative charge of mucus is provided by the mucin structure, consisting of a high content of sialic and sulfate moieties. Besides, mucin behaves like a polyampholyte, which is able to bind to hydrophilic and hydrophobic surfaces due to the presence of positively charged domains and hydrophobic amino acid residues.[41]

2.4.1. Scanning Electron Microscopy (SEM). A 0.04% w/v PGM stock dispersion in PBS (pH 6.8) was prepared under stirring at room temperature overnight. Then, 5 mL of the stock dispersion of PGM was mixed with 1 mL of 40 mg/mL of the empty NPs or RIF/ASC NPs. Mixtures were allowed to reach equilibrium for 24 h at 37 °C and 180 rpm in an orbital stirring. Aliquots of the mixtures were transferred into silicon slices adhered to a double-sided tape on suitable support for SEM, dried at 30 °C, and sputter-coated with gold to be imaged by SEM (SUPRA 40 (ZEISS)).

2.4.2. Rheology. Effects of NPs on PGM were investigated. Shear viscosity (η_{shear}) changes were determined as a function of shear rate (γ) of 3% w/v PGM aqueous dispersions at pH 6.8, incubated with empty NPs 1% w/v and RIF/ASC-loaded NPs 1% w/v in PBS at pH 6.8. Experiments were performed on a Rheoplus MCR 301 rheometer equipped with cone−plate CP50−1 geometry (diameter, 49.956 mm; cone angle, 1.006°) at room temperature. Samples were incubated under stirring at 180 rpm in an orbital stirring (Ferca, Buenos Aires, Argentine) at 25, 34, and 37 °C, for 30 min prior to rheological measurements.

2.4.3. Determination of Interactions between NPs and PGM Using Dynamic Light Scattering (DLS). Interactions between NPs and PGM were determined by adding 1 mL of suspensions containing 1 mg of empty NPs or RIF/ASC-loaded NPs in PBS (pH 6.8) to 1 mL of a 0.04% PGM dispersion in PBS (pH 6.8). Subsequently, mixtures were incubated under 180 rpm in an orbital shaker, at 37 °C, for 30 min. Subsequently, the mean size, ζ potential, and polydispersity index (PDI) of the dispersions were measured with a photon correlation spectroscopy (PCS) using a DLS.

2.5. Cytotoxicity of RIF/ASC NPs. *2.5.1. Cell Lines.* In order to evaluate the potential cytotoxicity of NPs on lung cells, A549 and MRC5 cells were incubated with increasing concentrations of free RIF, empty NPs, and RIF/ASC-loaded NPs for 5 and 24 h followed by the MTT assay.

The human cell line A549 is of alveolar origin, and it is routinely used *in vitro* as a surrogate for human pneumocytes because A549 cells share many properties with human respiratory cells.[42] Due to the large number of fibroblasts found in the lungs, we evaluated the human fetal lung fibroblasts MRC5 as a model of the subjacent connective tissue in the lungs.[43,44]

A549 (human lung adenocarcinoma) and MRC5 (normal lung fibroblast) cell lines were provided by ATCC (Virginia, USA). Both cell lines were cultured in Dulbecco's modified Eagle medium (DMEM, Gibco, USA) supplemented with 10% fetal bovine serum (FBS, Gibco, USA), 4 mM L-glutamine (Gibco, USA), 4 mM sodium pyruvate (Sigma-Aldrich, USA), and 10 000 UI/mL of penicillin/streptomycin and incubated at 95% humidity and 5% CO_2 at 37 °C.

2.5.2. MTT Cytotoxicity Assays. The cytotoxicity of free RIF, RIF/ASC NPs, and empty NPs was monitored by the MTT (3-(4,5-dimethylthiazol-2-yl)-2,5-diphenyl tetrazolium bromide) assay. Empty NPs suspensions were prepared by weighing equivalent amounts of unloaded NPs to those of NPs loaded with RIF/ASC, and corresponding dilutions equivalent to each concentration were made.

Initially, A549 (10 000 cells/well) and MRC5 (10 000 cells/well) cells were seeded in 96-well microplates in supplemented DMEM and allowed to grow until ∼80% of confluence. Next, cells were treated with 100 μL/well of each formulation and incubated for 5 and 24 h at increasing concentrations from 5 to 400 μg/mL. After treatment, cells were rinsed twice with 100 μL of PBS, pH 7.4 at 37 °C. Then, 100 μL/well of 250 μg/mL of yellow tetrazolium salt MTT solution in PBS was added per well and incubated for 30 min at 37 °C. After the incubation period, 200 μL of isopropanol solution was added to each well to solubilize the purple Formosan crystals formed by the cellular reduction of pyridine nucleotide cofactors NADH and NADPH in metabolic active cells. The resulting colored solution was quantified using a microplate reader (BioTek EL800, USA). The absorbance was measured at 560 nm. Results are expressed as the percent of cell viability reduction ± SD of values collected in comparison with the control samples (cells treated with vehicle). The percentage of growth inhibition was calculated according to the following equation:

$$\text{percentage viability} = \frac{\text{mean OD of samples} \times 100}{\text{mean OD of the control group}} \quad (3)$$

where OD is the optical density, which represents the absorbance values of the samples. The control OD arbitrarily represents 100%.

A 70% cutoff line was settled for acceptable cell viability in all treatments and concentrations evaluated on the basis of the ISO 10993-5 international guide, which declares a reduction in cell viability of 30% as the cytotoxic threshold.[45,46]

2.6. Pulmonary Delivery of Fluorescent Nanoparticles FITC (NPs-FITC). *2.6.1. Animals.* Animal experiments were approved by the Institutional Animal Care and Use Committee of the Instituto Ferreyra (CICUAL-IMMF). Male and female Wistar rats (∼400 g, 8 weeks old) obtained from the vivarium of the Instituto Ferreyra (INIMEC−CONICET-UNC, Córdoba, Argentina) were used in this study. Animals were housed in cages with 12 h light/dark cycles and free access to water and standard rodent food. Two rats (male and female) were assigned to each group.

2.6.2. Intratracheal Instillation of NPs-FITC. First, empty NPs were labeled with the isothiocyanate fluorophore, FITC

https://dx.doi.org/10.1021/acs.molpharmaceut.0c00692
Mol. Pharmaceutics 2021, 18, 807−821

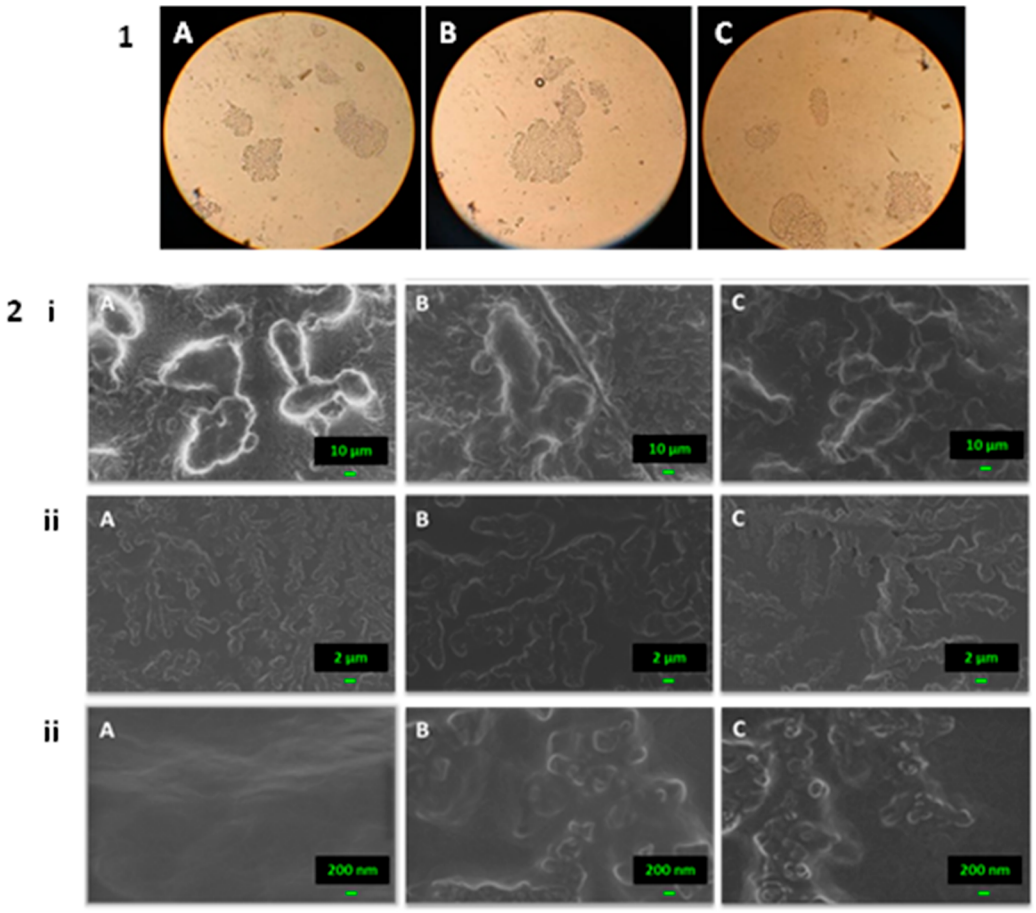

Figure 2. Optical microscopy images of (1) (A) PS, (B) PS with empty NPs, and (C) PS with RIF/ASC NPs at 60× magnification and (2) SEM images of (A) PS, (B) PS with empty NPs, and (C) PS with RIF/ASC NPs. Scale: (i) 10 μm, (ii) 2 μm, and (iii) 200 nm.

(Molecular Probes TM, Sweden), the NPs-FITC, as previously described.[29]

Wistar rats of both sexes were used for lung biodistribution studies and to identify the cells participating in the NPs uptake. Rats received an intratracheal instillation of a NP suspension previously labeled with FITC. At different times during postadministration, we collected the lung right superior and accessory lobe (RSL + AL), right middle and right inferior lobe (RML + RIL), left lobe (LL), and total spleen. The NP distribution in the lung sections and cellular uptake of nanoparticles were analyzed based on FITC expression by FACS.[47,48]

Rats were first anesthetized by inhalation of isoflurane and left to rest in the supine position. Upon holding the rat's tongue in extension, a catheter was introduced through the mouth into the throat up to the bifurcation of the trachea. Immediately after, the rat was held at 90 deg with respect to the normal walking position, and 600 μL of a saline solution (control) or an NPs-FITC suspension (1 mg/mL) was gradually dripped into the trachea using a Hamilton syringe. Rats were euthanized at 2, 4, 12, 24, and 48 h time points by CO_2 asphyxiation. Immediately after euthanasia, the thorax of the rats was opened, and the lungs and spleen were excised. To eliminate the excess of NPs that did not reach the lung cells, the airways were first washed through the trachea with 2 mL of saline solution. The liquid was let go without aspirating it. Three lobes of the right lung were processed separately: right superior lobe (RSL), accessory lobe (AL), and right inferior lobe (RIL). The left lung was processed in one piece. Samples were then analyzed by flow cytometry in order to analyze the pulmonary distribution of NPs-FITC.

2.6.3. Flow Cytometry (FACS). Single-cell preparations were obtained from lung sections and the spleen of rats by passing them across a 100 μm cell strainer to disaggregate the tissue. To carry out this procedure, the cell strainers were placed in six-multiwell plates containing the portions of each organ with 4 mL of physiological solution. Pressure was applied with the plunger of a plastic syringe to disaggregate the tissue, and subsequently, the cell suspension was extracted and transferred to Falcon tubes. Erythrocytes were removed from cell suspensions by addition of 4 mL of red blood cell lysis solution (NH_4Cl 150 mM, $KHCO_3$ 10 mM, and Na_2EDTA 0.1 mM) and centrifuged at 2000 rpm for 5 min. Cells were then washed with a staining buffer (PBS + 2% FBS). Dissociated cells were incubated with a mix of anti-CD11bPerCP.Cy5.5 (CAT, 45−0112−82, eBioscience) and anti-F4/80-PECy7 (CAT, 123114, Biolegend) monoclonal antibodies. Double positive F4/80+CD11b+cells were identified as macrophages. Flow cytometry analysis was performed on a BD FACS Canto II system. The data was analyzed using FlowJo_V10 software.

2.6.4. Immunofluorescence Microscopy. The qualitative location of empty NPs labeled with the fluorescent biomarker FITC (NPs-FITC) was assessed by using immunofluorescence confocal microscopy as previously described.[29] Macrophage identification was performed by their immunoreactivity to the CD64 primary antibody (bs-3511R, Bioss Antibodies).[49,50]

https://dx.doi.org/10.1021/acs.molpharmaceut.0c00692
Mol. Pharmaceutics 2021, 18, 807−821

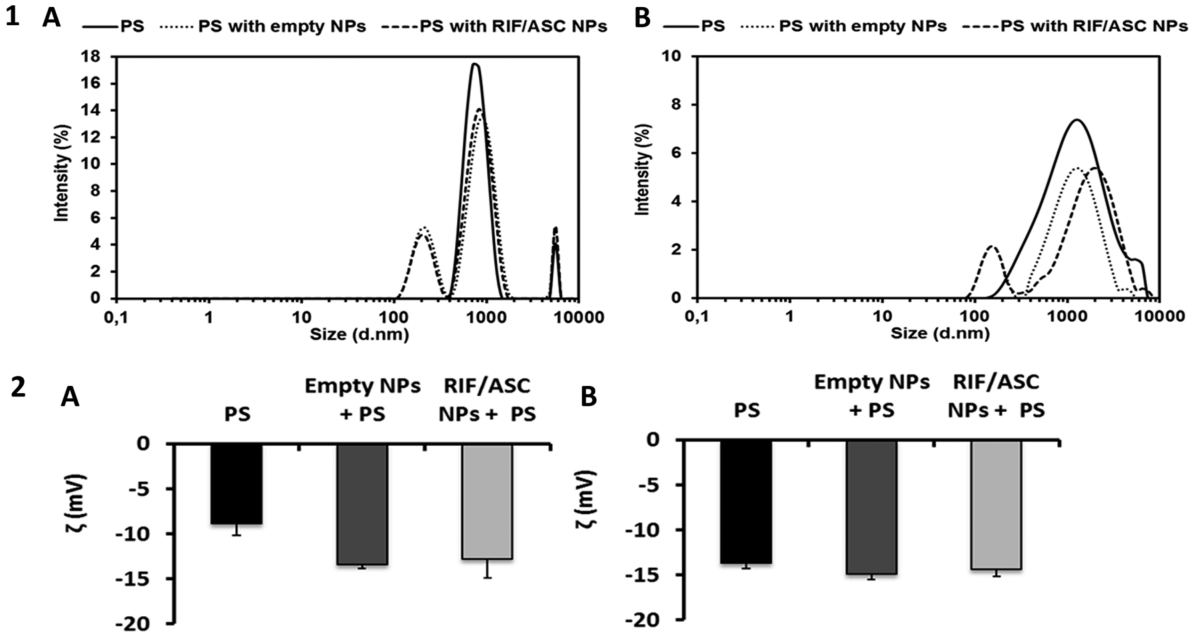

Figure 3. (1) Size distribution by intensity (%) of PS, PS with empty NPs, and RIF/ASC NPs at (A) 5 h and (B) 24 h. (2) Variation of ζ potential of PS with empty NPs and RIF/ASC NPs at (A) 5 h and (B) 24 h.

To this end, one rat was instilled with a saline solution (control), and three rats were instilled with FITC-labeled NPs. Then, two rats were sacrificed after 2 h (NPs-FITC 2 h) and the others after 4 h (control and NPs-FITC 4 h). The lungs were isolated and fixed in a 4% paraformaldehyde (PFA) solution overnight at room temperature. Lungs were placed in a 15% sucrose solution after PFA withdrawal and stored at 4 °C until processing. Left lungs were separated, and tissues were embedded in the Tissue-tek OCT compound (Sakura Torrance, CA). Lung sections of 10 μm were obtained by using a Leica CM1850 cryostat (Leica, Germany). Briefly, lung sections were hydrated with water for 15 min, followed by permeabilization with a buffer containing 0.3% Triton X-100 and 5% bovine serum albumin (BSA) in PBS for 1 h. After two washes with a washing solution containing 0.1% tween 20 and 0.2% of BSA, an anti-CD64 primary antibody was incubated overnight in the washing solution at 4 °C. Next, the slides were washed five times with a washing solution, and the secondary antibody (Invitrogen) was added and incubated for 1 h at room temperature. Then, the tissue was washed five times with a washing solution, and nuclei were stained with DAPI (4′,6-diamidino-2-phenylindole). Next, the coverslips were treated with 8 μL of Prolong Gold (Thermo Fisher Scientific) and mounted onto glass slides. The preparations were preserved in the dark and stored at 4 °C for 24 h.[51] Subsequently, confocal images were acquired using an FV 1200 fluorescence confocal laser microscope (Olympus).

2.7. Statistics Analysis. Data are presented as means ± standard deviation (SD) from at least two independent experiments. All data were analyzed using one-way ANOVA with the least significant difference and *t*-student test at a defined level of statistical significance of $p < 0.05$.

3. RESULTS

3.1. Interactions between RIF/ASC-Loaded NPs and PS. Figure 2 shows images taken under an optical microscope displaying the molecular organization of PROSURF-B alone or after its incubation with empty NPs or RIF/ASC-loaded NPs. Figure 2.1.A reveals the presence of surfactant clusters with occasionally associated vesicles and small spherical surfactant aggregates. Remarkably, the addition of either empty NPs or RIF/ASC-loaded NPs to the surfactant dispersion did not produce any significant change in the microstructure of PROSURF-B (Figure 1.1.B,C).

Next, scanning electron microscopy (SEM) was used to visualize the surface topology of the surfactant and to locate the NPs in the PS layer. The SEM image of the PS model without NPs (Figure 2.2.A) shows the presence of large filamentous and disclike structures, corresponding probably to protein-induced lipid multilayer assembly into larger micrometric structures.

Figure 2.2.B,C shows that both empty NPs and RIF/ASC-loaded NPs did not substantially affect the structural organization of the PS. Besides, the presence of NPs closely associated with the surface-surfactant structures without causing any significant change in the morphological characteristics of the surfactant structural organization is observed in these figures.

The particle size distribution (PSD) pattern of the PROSURF-B dispersion alone (Figure 3.1.A), at 5 h, showed a bimodal distribution, where the major maximum average hydrodynamic size peak was ∼1000 nm along with a small peak with a maximum average size of ∼8000 nm. The broad size distribution of the mainly maximum hydrodynamic size peak (Figure 3.1.B), extended from 150 to 8600 nm after 24 h, suggested that the surfactant particles started to aggregate, fuse, and coarsen. Interestingly, the DLS patterns of the PROSURF-B dispersion obtained after 5 and 24 h of lung surfactant incubation with either the empty NPs or RIF/ASC-loaded NPs showed similar characteristics to those found with the surfactant alone in the same incubation periods; they indicated that the NPs did not produce any effect on the DLS behavior pattern of the lung surfactant. In these last experiments, it was also visible a peak with an average maximum size of ∼200 nm attributed to the NPs. In agreement with these results, the microscopic studies showed that NPs allow the surfactant to

https://dx.doi.org/10.1021/acs.molpharmaceut.0c00692
Mol. Pharmaceutics 2021, 18, 807−821

maintain its structural integrity but trapping the NPs on its surface without altering the biophysical structural organization of the lung surfactant film; hence, NPs may be considered compatible with the biophysical function of the PS.

Figure 3.2.A,B shows the local electrical potential (ζ potential) of dispersions of the extracted bovine lungs surfactant PROSURF-B, alone or after its incubation with empty NPs or RIF/ASC-loaded NPs. The ζ potential of the surfactant aggregates was found to slightly change from values of near −10 mV to values close to −15 mV, after both 5 and 24 h of incubation. The overall negative ζ potential of the PS dispersions alone at both times may be attributed to the high proportion of saturated zwitterion or negatively charged phospholipids in combination with a small proportion of hydrophobic proteins positively charged. The ζ potential of the PROSURF-B dispersions correlated with previous reports in the literature.[52]

For the maintenance of the PS function, it is relevant that the NPs preparations do not show significant surface activity. Surface tension measurements were performed for different subphase concentrations of empty or RIF/ASC-loaded NPs in comparison with a bare buffer surface (Figure 4). We observed

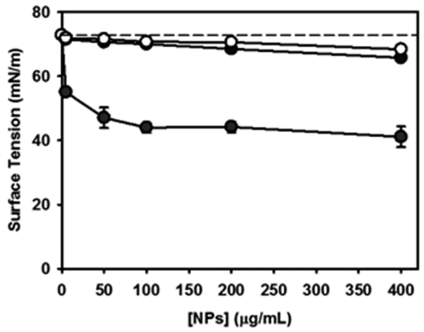

Figure 4. Surface tension of empty NPs (white symbols) or with RIF/ASC-loaded NPs (black symbols), as a function of subphase concentration. The surface tension of a T80 solution of a concentration equivalent to the present in NPs preparations was also plotted (gray symbols). The horizontal dashed line represents the surface tension of the clean buffer surface. Data is the mean of two experiments, and error bars are SD. When no error bar is observed, it is smaller than the size of the symbol.

a reduction of 6 and 10% of surface tension when 400 μg/mL of empty or RIF/ASC-loaded NPs were present at the subphase, respectively. Additionally, we explored the effect of T80 on surface tension in a concentration range equivalent to that present in the NPs formulations. An important reduction (44%) of surface tension was found for the maximal T80 concentration explored. This suggests that the detergent molecules present in the NPs formulation remain strongly adsorbed to the NP structure and scarcely interact with the air−buffer surface, preserving the surface physical properties.

To explore the tendency of RIF/ASC NPs to interact with PS, we constructed PS monolayers onto the air−buffer surface (at a surface pressure of 25 mN/m) and added fluorescent NPs (NPs-FITC) to the subphase (200 μg/mL). No further increase in surface pressure was observed after the addition of the NPs (not shown). We also recollect by aspiration the surface fraction and compare its fluorescent intensity with that of the subphase fraction. No enrichment of NPs-FITC was found within the sensibility of the technique. Those tests support that when NPs are exposed to a PS film, they do not undergo adsorption or accumulation at the surface.

Furthermore, the effect of empty NPs and RIF/ASC-loaded NPs on the surface organization of PS films was explored. Isothermal compression and simultaneous visualization experiments were performed by Brewster angle microscopy (BAM). Figure 5 shows BAM images of PS films, which were compressed up to a surface pressure of 10 mN/m and subjected to the addition at the surface of empty or RIF/ASC-loaded NPs, to reach a surface concentration of 130 μg/cm^2. This concentration results from considering the dosage used for rat experiments (600 μg NPs/animal) and the estimated alveolar surface per animal (82.2 cm^2).[53]

PS films show a uniform gray surface at low surface pressures (<10 mN/m, not shown), which corresponds to a liquid-expanded phase and the nucleation and growth of light gray domains above this pressure (Figure 5). An increase in the gray level of BAM images corresponds to an increase in the thickness and/or the refraction index of the film. In the case of PS, the bright domains correspond to a liquid-condensed dispersed phase enriched in the main component of PS: dipalmitoylphsphatidylcholine.[54,55] The addition of empty NPs or RIF/ASC-loaded NPs to the PS monolayer did not alter its surface topography (Figure 5) or the shape of the compression isotherms (not shown). On the contrary, the addition of T80 in a concentration equivalent to that present in the NP formulation induced the reduction of the condensed domains and a shift of their nucleation to higher surface pressures. This effect is evidence of stabilization of the liquid-expanded phase by the detergent, altering phase equilibrium.[55] Again, those results show that T80 does not disturb the surface structure when incorporated into the NPs.

3.2. Interactions of Empty NPs and RIF/ASC-Loaded NPs with Pig Gastric Mucin (PGM) as a Lung Mucus Model.

Figure 6.1 shows that the PSD curve of the PGM alone was monomodal, with a maximum hydrodynamic radius at 615 nm attributed to the formation of large aggregates of mucin. When either empty NPs or RIF/ASC-loaded NPs were added to the PGM dispersion, the monomodal PSD curve of mucin changed into bimodal curves, showing that, after mixing PGM with the NPs, the maximum hydrodynamic peak of the PGM shifted toward lower values, at 531 nm for the PGM-empty NP mixture and at 459 nm for the PGM-RIF/ASC-loaded NP mixture (Figure 6.1). Additionally, it was noted, in the PSD curves obtained after mixing PGM with either the empty NPs or the RIF/ASC-loaded NPs, a lower and weaker hydrodynamic peak at 78.8 nm or at 91.3 nm, respectively, attributed to small species. On the other hand, the hydrodynamic size peak corresponding to both NP suspensions was not detectable, probably because of associative interactions between PGM and NPs.

The PGM behavior upon adding the NPs was also translated into macroscopic rheological changes as illustrated by the slight increase in the viscosity of the dispersions of PGM in the presence of NPs, as shown in Figure 6.2. However, the addition of the NPs was not able to change the viscosity of PGM significantly, suggesting that the nature of the interaction between PGM and NPs was weak.

The lack of disturbance of the rheological properties of the PGM after contacting the NPs was also reflected in the SEM images obtained from the PGM-NP mixtures (Figure 6.3), revealing that the microstructure of PGM was minimally perturbed after establishing contact with the NPs. From these

https://dx.doi.org/10.1021/acs.molpharmaceut.0c00692
Mol. Pharmaceutics 2021, 18, 807−821

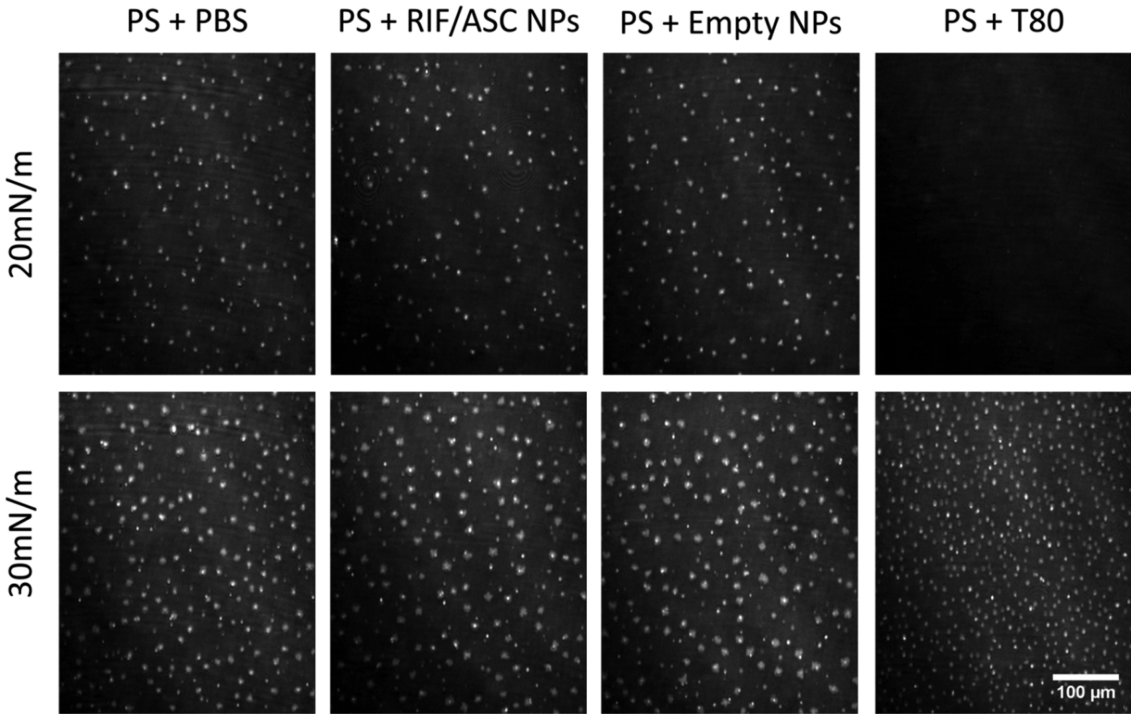

Figure 5. BAM images of PS with empty NPs, RIF/ASC-loaded NPs, and control experiments as indicated, at a surface pressure of 20 or 30 mN/m. NP surface concentration = 130 $\mu g/cm^2$. The images are representative of duplicated experiments.

results, it was inferred that, despite the fact that NPs seem to associate preferentially on the PGM surface, PGMs' fibers appeared to be hydrated, highly elongated, and rodlike or wormlike randomly oriented. This reassembles PGM in the absence of the NPs.

These results allowed us to hypothesize that both hydrophilicity and entropic repulsive properties of NPs prevent the strong adsorption of the NP to mucus components, which would facilitate the unhindered diffusion-based transport of the NPs through the mucus because it is unlikely that electrostatic interactions between PGM and NPs occur as shown by the ζ potential results (Figure 7).

3.3. Evaluation of Cell Cytotoxicity of RIF/ASC NPs. The effects of different formulations on the *in vitro* viability of A549 and MRC5 cells are shown in Figure 8.

Results showed that both cell lines preserved viability superior to 90% after 5 h of treatment with either the empty NPs or the RIF/ASC-loaded NPs at all concentrations used (Figure 8A,B). Viability was lower than 90% in A549 cells when incubated with free RIF at concentrations higher than 100 μg/mL (Figure 8A). After 24 h of treatment, RIF/ASC-loaded NPs did not significantly decrease cell viability except at the highest concentration (400 μg/mL), in which viability dropped to about 70% in both cell lines (Figure 8C,D). Conversely, cell viability was significantly reduced and beneath 70% at concentration with free RIF above 100 μg/mL, indicating high cytotoxicity in both cell lines (Figure 8C,D). Interestingly, the viability was over 90% after empty NP treatment at all tested concentrations in both cell lines, revealing that empty NPs were noncytotoxic, which, combined with our previous results, make this suspension biocompatible (Figure 8).

3.4. NPs-FITC Distribution and Identification of Cells Participating in Their Uptake in the Lungs. A higher accumulation of NPs was observed at early stages (2, 4, and 12 h), which decreased after 24 and 48 h postadministration to the lungs (Figure 9). No significant differences were observed between sections of this organ. In addition, NPs were undetectable in the spleen, suggesting that the particles do not recirculate in the blood (Figure 9).

Previously, we have reported that after intratracheal administration, NPs are found in cells similar to macrophages when the lungs are observed by immunofluorescence.[29] Taking into account that macrophages are recruited to capture different agents at the tissue level, these cells were studied by FACS at different times after administration. Macrophages were identified as F4/80+ CD11b+, and their ability to capture NPs was registered by FITC. Figure 10 demonstrates macrophage recruitment after administration. An increase in the percentage of macrophages was observed (Figure 10A) concurrently with NP accumulation (2, 4, and 12 h) in Figure 9. After 24 h postadministration, the macrophages return to basal levels indicating that their recruitment is promoted by NPs.

To evaluate their capacity to capture NPs, the expression on F4/80+ CD11b+ cells (Figure 10B) and mean intensity fluorescence (MFI, Figure 10C) of FITC were studied. About 50−70% of macrophages uptake NPs, after early times postadministration, and gradually decrease to 20−30% at 24 h or less than 10% at 48 h. In concordance, MFI of FITC in macrophages is higher at early times postadministration and decreases at longer periods (Figure 10C). It is important to highlight that macrophages did not recirculate, indicated by the absence of both free FITC+ and macrophages FITC+ in the spleen. Finally, the proportion of FITC+ cells expressing macrophage markers was evaluated to confirm that around 80−100% of the cells capturing NPs correspond to this population (Figure 10D). NPs were found in the alveolar space at both 2 h (Figure 10E) and 4 h (Supplementary Figure B) within the tissue. NPs were also observed in the bronchi

https://dx.doi.org/10.1021/acs.molpharmaceut.0c00692
Mol. Pharmaceutics 2021, 18, 807−821

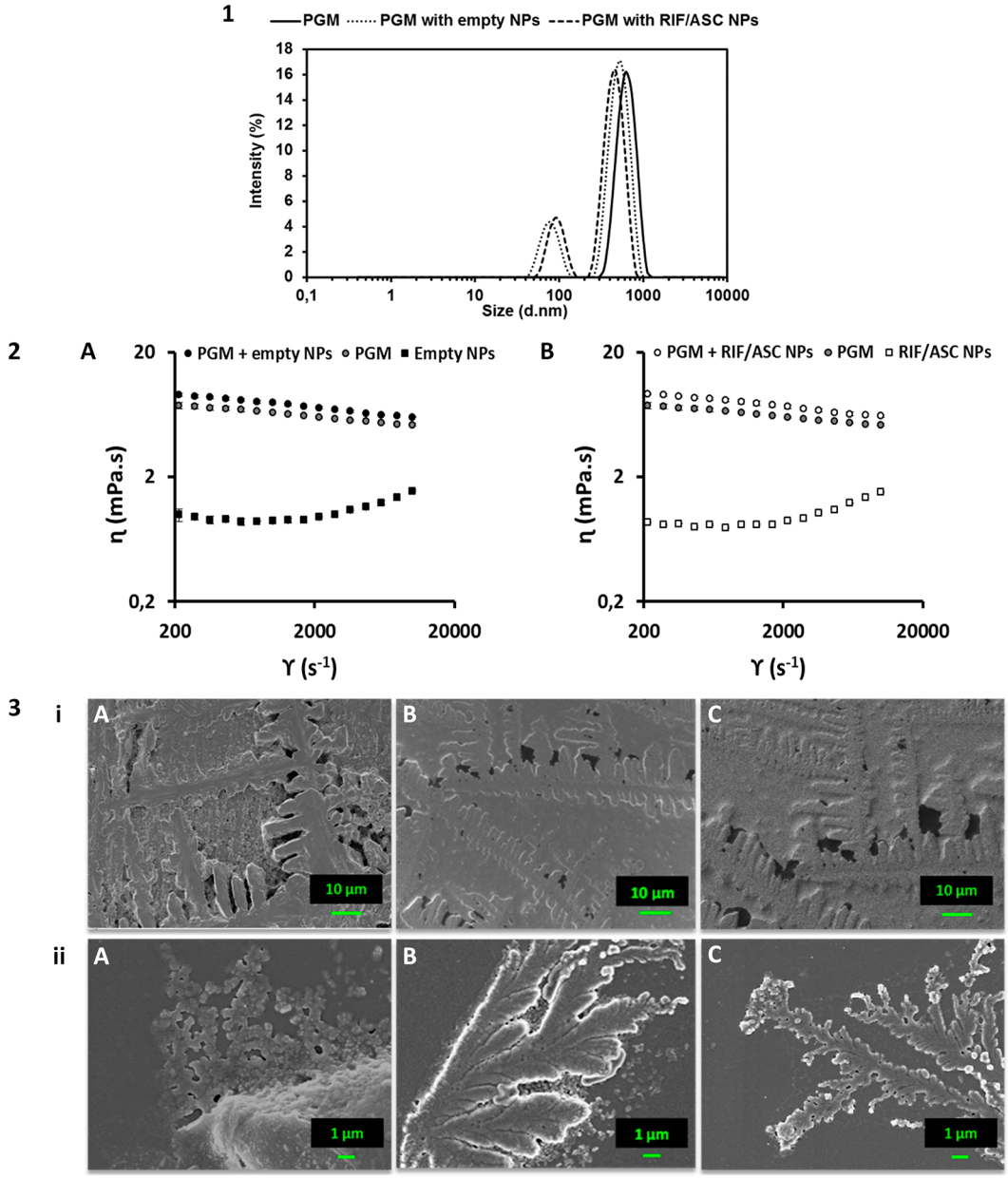

Figure 6. (1) Size distribution by intensity (%) of PGM, PGM with empty NPs, and RIF/ASC NPs. (2) Viscosity behavior of PGM, empty NPs, and PGM with empty NPs and PGM, RIF/ASC NPs, and PGM with RIF/ASC NPs. (3) SEM images of (A) PGM, (B) PGM with empty NPs, and (C) PGM with empty NPs and RIF/ASC NPs. Scale: (i) 10 μm and (ii) 1 μm.

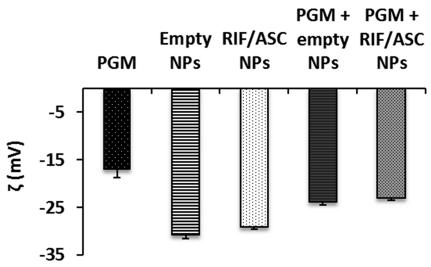

Figure 7. Variation of ζ potential of PGM (0.04% w/v) with empty NPs and RIF/ASC NPs (1 mg/mL).

(Supplementary Figure C and D). As expected, NPs were found either free or inside of cells expressing the macrophage marker CD64, as shown in immunofluorescence (Figure 10E). In concordance with FACS data, immunofluorescence assays confirmed that macrophage recruitment in the lungs was higher at 2 h (Figure 10E) and 4 h (Supplementary Figure B) in NPs-FITC-instilled compared to control saline-instilled rats. Taken together, these results indicate that NPs are distributed homogeneously in the lungs and almost exclusively captured by recruited macrophages.

4. DISCUSSION

In this work, we explored the directly inhaled formulation of a novel CS and T80-decorated ALG nanocarrier encapsulating the antibiotic RIF with an antioxidant ASC previously developed for the treatment of respiratory intracellular infections. To this end, we investigated the effects of RIF/ASC-loaded NPs on the respiratory mucus and the PS, their potential cytotoxicity for lung cells *in vitro*, and their

https://dx.doi.org/10.1021/acs.molpharmaceut.0c00692
Mol. Pharmaceutics 2021, 18, 807−821

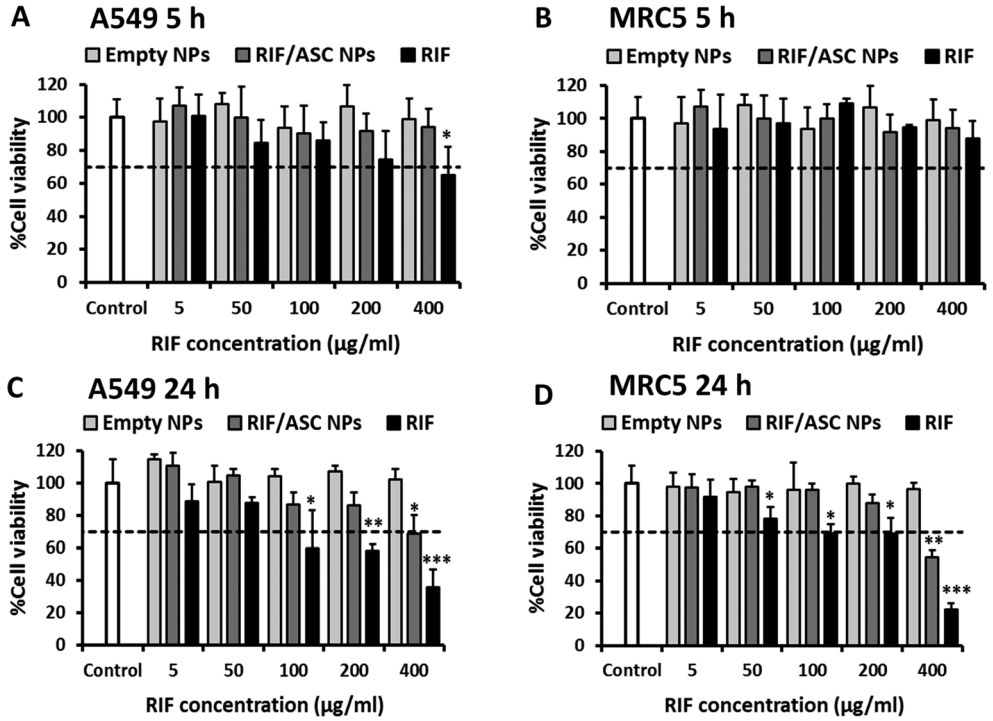

Figure 8. *In vitro* cytotoxicity of RIF, empty NPs, and loaded RIF/ASC NPs in the (A) A549 cell line at 5 h, (B) MRC5 cell line at 5 h, (C) A549 cell line at 24 h, and (D) MRC5 cell line at 24 h (mean ± SD, $n = 3$, * p-value < 0.05, ** p-value < 0.01, *** p-value < 0.001). RIF/ASC NPs contain an amount of RIF equivalent to free RIF.

biodistribution in lungs *in vivo*. Additionally, we investigated the identity of cells that actively phagocytize them.

Several studies have shown that inhaled polymeric NPs adversely affect the biological function of the PS, which was attributed to the physicochemical characteristics of NPs; among these characteristics, the NP's surface charge is involved in this phenomenon.[56] The NP's surface functionalization is a promising strategy to improve the safety of NPs in the lungs through the tuning of the surface of NPs in order to minimize the unwanted effects of polymeric NPs on the biophysical function of PS.[47] In this study, RIF/ASC-loaded alginate NPs were functionalized with CS and the nonionic surfactant T80. In our previous report, CS and T80 provided special surface-active properties to the ALG NPs loaded with the RIF/ASC, producing the so-called "glycocluster effect" and a protective shell on the surface of NPs, which gives them a greater hydrophilic character.[28,29] Based on these considerations, studies were focused on determining the effects of both empty NPs and RIF/ASC-loaded NPs on the lung surfactant model (PROSURF-B) particles evolution behavior by assessing PSD, the surface ζ potential of these systems, and microscopic studies. Accordingly, findings shown herein lead to infer that the specific coating qualities of the RIF/ASC-loaded NPs are capable of efficiently shielding from perturbation of the normal lung surfactant function. On the other hand, the mucus lining in the airways also may be a barrier against NPs intended as inhaled therapeutic drug carriers because therapeutic systems are hindered in overcoming this thick and highly viscous mucus barrier to reach the target side.[57] Respiratory mucus behaves like a non-Newtonian fluid with special rheological properties directly affecting its clearance ability. Since mucin mainly drives the typical viscoelastic behavior of mucus through reversible and irreversible associations across its *O*-glycosylated polypeptide chains,[58] in this study, a PGM was used as a respiratory mucosal barrier model to assess biophysical interactions between mucin and empty NPs or RIF/ASC-loaded NPs. Specifically, we investigated the changes in the rheological properties and the microscopic gel structure of mucin exposed to the NPs. The results obtained indicate that RIF/ASC-loaded NPs are muco-inert and potentially able to penetrate the airway mucus layer and later be internalized by cells in the lung, as we have shown in the *in vivo* experiments.

In concordance with the above results and, as expected, the analysis of viability in two different lung-related cell types, A549 and MRC5, showed that empty NPs did not alter cell metabolism in any of the evaluated time points and concentrations, indicating that NPs are not cytotoxic for lung cells *in vitro*. Interestingly, RIF/ASC-loaded NPs displayed much higher viability than the one produced by RIF alone, at an equivalent range of concentration. Although further experiments should be performed to investigate the potential cytotoxicity of this formulation in AMs, these results demonstrated that RIF/ASC-loaded NPs have both a good biocompatibility and are safer than pure RIF.

In order to describe the distribution of RIF/ASC-loaded NPs in the target organ, *in vivo* administrations were performed by intratracheal instillation in rats. The results showed a homogeneous distribution of NPs in all sections of the lungs. NPs are mostly located in both the alveolar space and in bronchus as previously observed.[29] Under different conditions, bone marrow-derived monocytes can be recruited to lungs and then differentiated into AMs.[59,60] We have demonstrated that NPs administered directly to lungs induce the recruitment of monocyte-derived macrophages F480+ CD11b+. However, about 15% of NPs+ cells did not express markers of these populations, indicating that phagocytes as other immune cells (eosinophils, neutrophils, dendritic cells),

https://dx.doi.org/10.1021/acs.molpharmaceut.0c00692
Mol. Pharmaceutics 2021, 18, 807−821

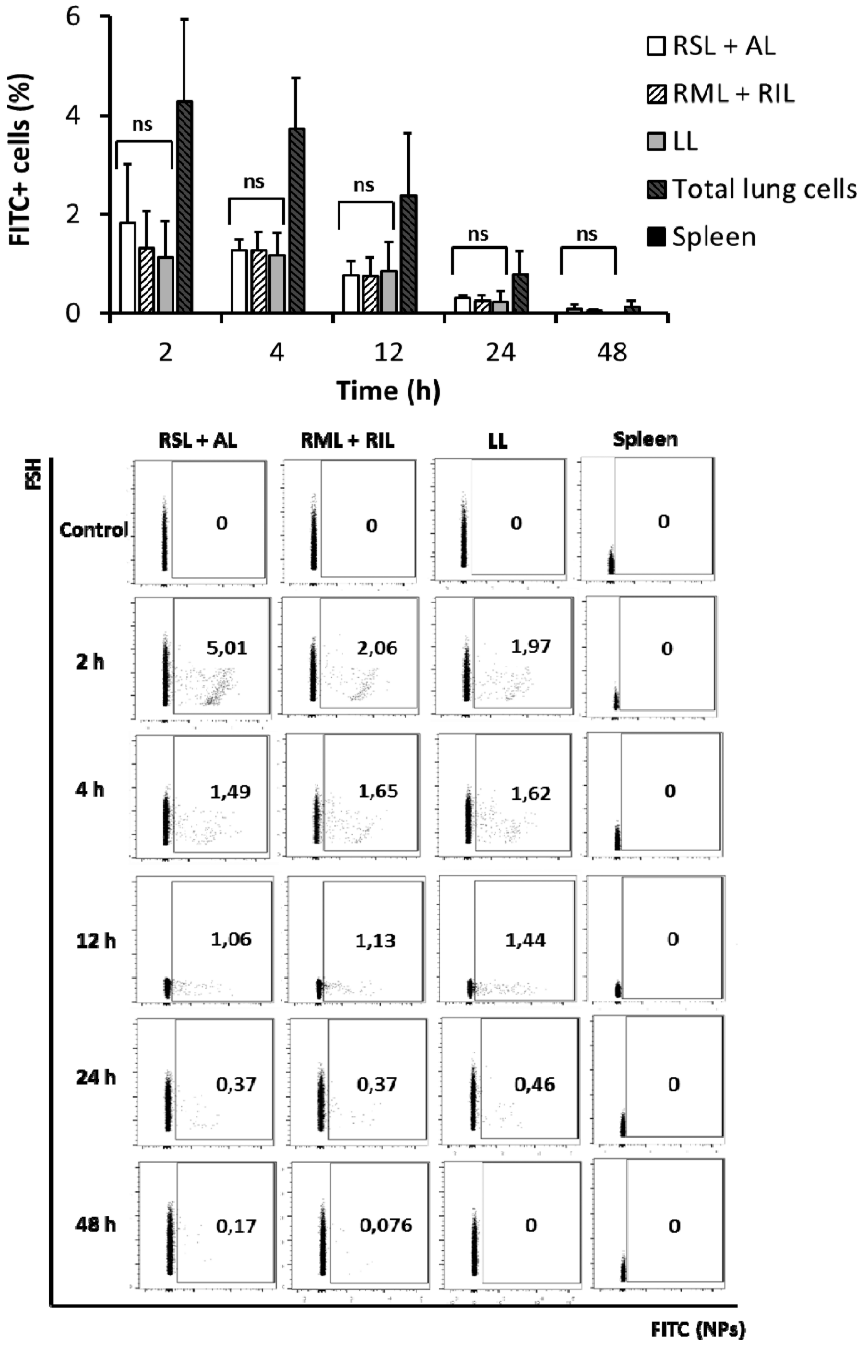

Figure 9. NPs are homogeneously accumulated in the lungs after intratracheal instillation. Rats at each time point (n = 2) were administered intratracheally with NPs-FITC. After 2, 4, 12, 24, and 48 h NPs into cells (cells FITC+), the distribution of NPs-FITC was evaluated by FACS in different lung sections and spleen (mean ± SD, n = 2, ns: no significant difference): RSL+AL (right superior and accessory lobes), RML+RIL (right medium and inferior lobes), LL (left lobe). Total lung cells were obtained from the summation of the different sections of the lungs.

fibroblast, epithelial, or endothelial cells, could uptake NPs. Macrophages are professional phagocytes trained in the recognition, ingestion, and elimination or presentation to the adaptive immune system of particles, microbes, and apoptotic cells. An increase in FITC MFI (NPs) was observed in macrophages at early times compared with MFI at later times during postadministration, indicating that these cells could uptake, maintain the concentration over time and also metabolize NPs. Currently, the possibility of generating drug delivery systems in an infectious context to the lungs is a special consideration. Taking into account that macrophages can (1) uptake and metabolize NPs and (2) act as both host and effector cells for a large number of intracellular pathogens lodge in the lungs, this work allowed us to postulate NPs as an integral drug carrier system. According to our previous RIF release from NPs data, after 24 h, no release of RIF from NPs is observed, which means that NPs remain stable until they are taken up by cells, and therefore, it is highly probable that the drug will not be released from NPs until they are uptaken by cells and come into contact with the bacteria.[28,29]

Even though cytotoxicity experiments are aimed to determine the effects of the RIF/ASC NPs on the preservation of the viability of the main cells of the target tissue, it is important that the cytotoxicity of AMs should also be tested

https://dx.doi.org/10.1021/acs.molpharmaceut.0c00692
Mol. Pharmaceutics 2021, 18, 807−821

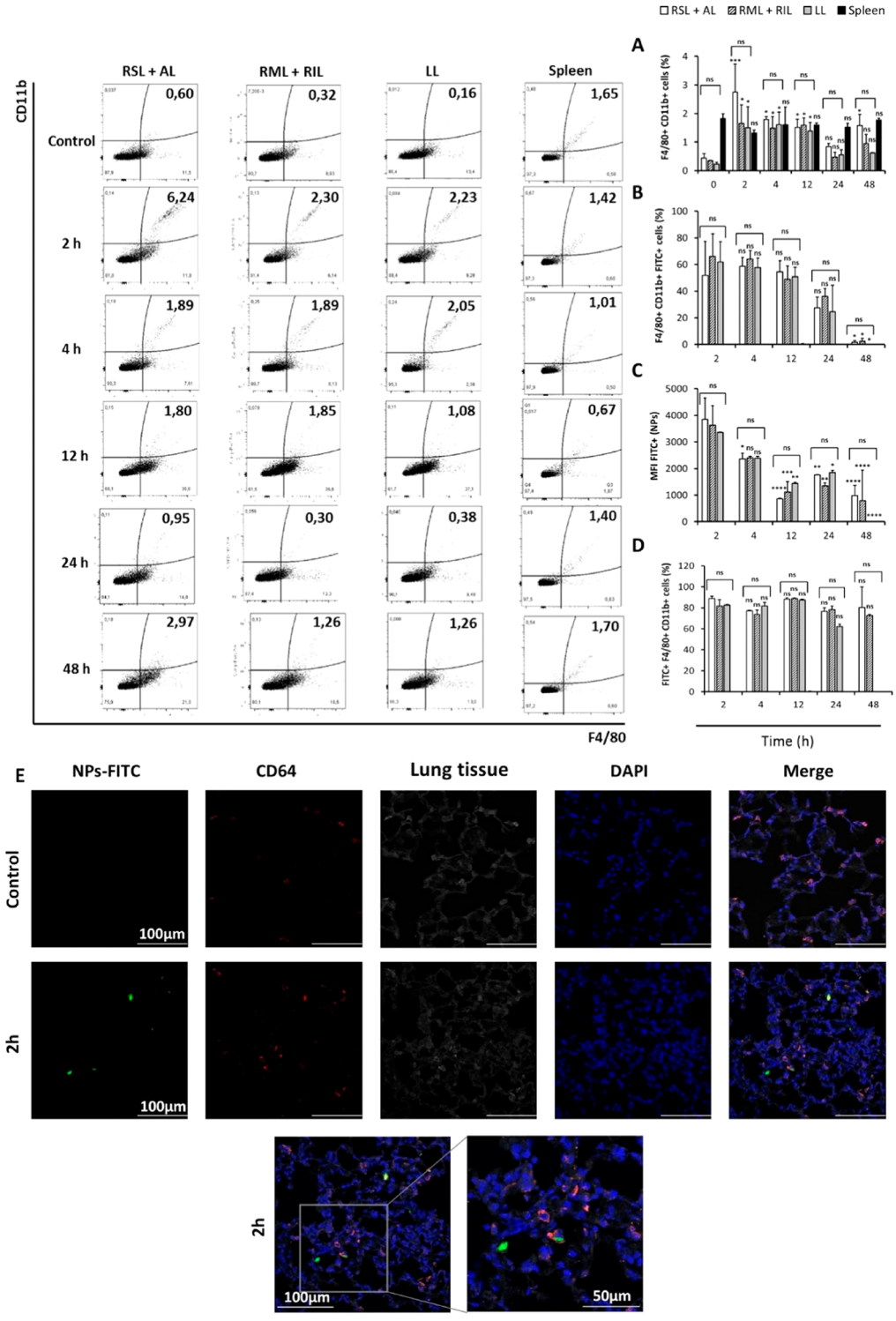

Figure 10. After administration, macrophages are recruited to the lungs and uptake NPs. Rats at each time point (n = 2) were administered intratracheally with NPs-FITC. After 2, 4, 12, 24, or 48 h, the recruitment and NP uptake (FITC) of macrophages (F4/80+ CD11b+) were evaluated by FACS in different lung sections and the spleen. The panels show (A) % of macrophages after instillation. For statistical analysis, ANOVA was applied using rats administered with the vehicle as a control. (B) Percentage of macrophages uptaking NPs. (C) Mean fluorescence intensity (MFI) of NPs in macrophage population. (D) Percentage of cells that are NPs+ and concomitantly express markers of macrophages. Statistics in parts B and C were calculated for every time point by ANOVA using 2 h postadministration as a control of positive NP accumulation in each section (mean ± SD, n = 2, ns: no significant difference, *p < 0.05, **p < 0.01, ***p < 0.001, ****p < 0.0001): RSL+AL (right superior and accessory lobes), RML+RIL (right medium and inferior lobes), and LL (left lobe). (E) Representative lung sections of the control and 2 h postinstillation of NPs-FITC (green), stained with CD64 (red) and DAPI (blue). Lung tissue was displayed for context by rising brightness levels in a duplicate of the CD64 channel. The bottom panels show a magnification of the 2 h lung section picture, where NPs-FITC can be observed both free and inside macrophages (CD64-stained cells).

https://dx.doi.org/10.1021/acs.molpharmaceut.0c00692
Mol. Pharmaceutics 2021, 18, 807−821

both *in vitro* and *in vivo* after NPs treatment. Moreover, important biological aspects should be additionally evaluated, such as the effectiveness of RIF/ASC-loaded NPs to resolve infections *in vivo*, type of immune response induced, inflammatory intermediaries involved, and cell metabolism changes in the response to NPs interaction. Therefore, further experiments should be performed to evaluate this formulation for its use in humans.

5. CONCLUSIONS

In summary, findings from this work show that our novel NPs encapsulating the antibiotic RIF with an antioxidant ASC based on ALG, using CS and T80 surface coating for functionalization, could be a suitable system for drug lung administration with promising perspectives for effective treatment of pulmonary intracellular infections.

■ ASSOCIATED CONTENT

Supporting Information

The Supporting Information is available free of charge at https://pubs.acs.org/doi/10.1021/acs.molpharmaceut.0c00692.

Stain images (PDF)

■ AUTHOR INFORMATION

Corresponding Authors

Melina M. Musri − *Instituto de Investigación Médica Mercedes y Martín Ferreyra, Consejo Nacional de Investigaciones Científicas y Técnicas, Universidad Nacional de Córdoba (INIMEC−CONICET-UNC), Córdoba X5000HUA, Argentina; Facultad de Ciencias Exactas Físicas y Naturales, Universidad Nacional de Córdoba, Córdoba X5000HUA, Argentina*; Phone: 54-351-4681465; Email: mmusri@immf.uncor.edu

Gladys E. Granero − *UNITEFA, CONICET and Departamento de Ciencias Farmacéuticas, Facultad de Ciencias Químicas, Universidad Nacional de Córdoba, Córdoba X5000HUA, Argentina*; orcid.org/0000-0003-2142-1675; Phone: 54-351-5353865-55315; Email: glagranero@unc.edu.ar

Authors

Ivana R. Scolari − *UNITEFA, CONICET and Departamento de Ciencias Farmacéuticas, Facultad de Ciencias Químicas, Universidad Nacional de Córdoba, Córdoba X5000HUA, Argentina*

Ximena Volpini − *Instituto de Investigación Médica Mercedes y Martín Ferreyra, Consejo Nacional de Investigaciones Científicas y Técnicas, Universidad Nacional de Córdoba (INIMEC−CONICET-UNC), Córdoba X5000HUA, Argentina*

María L. Fanani − *Departamento de Química Biológica Ranwel Caputto, Facultad de Ciencias Químicas, Universidad Nacional de Córdoba, Córdoba X5000HUA, Argentina; Centro de Investigaciones en Química Biológica de Córdoba (CIQUIBIC), CONICET, Córdoba X5000HUA, Argentina*

Benjamín De La Cruz-Thea − *Instituto de Investigación Médica Mercedes y Martín Ferreyra, Consejo Nacional de Investigaciones Científicas y Técnicas, Universidad Nacional de Córdoba (INIMEC−CONICET-UNC), Córdoba X5000HUA, Argentina*

Lautaro Natali − *Instituto de Investigación Médica Mercedes y Martín Ferreyra, Consejo Nacional de Investigaciones Científicas y Técnicas, Universidad Nacional de Córdoba (INIMEC−CONICET-UNC), Córdoba X5000HUA, Argentina*

Complete contact information is available at: https://pubs.acs.org/10.1021/acs.molpharmaceut.0c00692

Notes

The authors declare no competing financial interest.

■ ACKNOWLEDGMENTS

Authors acknowledge The Consejo Nacional de Investigaciones Científicas y Técnicas (CONICET), The Secretaría de Ciencia y Técnica de la Universidad Nacional de Córdoba (SECyT-UNC), and The Fondo para la Investigación Científica y Tecnológica (FONCYT) for providing the support and the facilities for this study. Also, authors thank Nialtec S.A. (Buenos Aires, Argentina), who generously provided us the surfactant PROSURF-B (lot 0432) as a gift. Authors also want to thank Dr. Anna Serrano-Mollar for her advice with the *in vivo* studies.

■ REFERENCES

(1) Momin, M. A. M.; Tucker, I. G.; Doyle, C. S.; Denman, J. A.; Sinha, S.; Das, S. C. Co-spray drying of hygroscopic kanamycin with the hydrophobic drug rifampicin to improve the aerosolization of kanamycin powder for treating respiratory infections. *Int. J. Pharm.* **2018**, *541*, 26−36.

(2) Siemer, S.; Westmeier, D.; Barz, M.; Eckrich, J.; Wünsch, D.; Seckert, C.; et al. Biomolecule-corona formation confers resistance of bacteria to nanoparticle-induced killing: Implications for the design of improved nanoantibiotics. *Biomaterials* **2019**, *192*, 551−559.

(3) Forum of International Respiratory Societies. *The Global Impact of Respiratory Disease*, 2nd ed.; European Respiratory Society: Sheffield, 2017.

(4) Troeger, C.; Forouzanfar, M.; Rao, P. C.; Khalil, I.; Brown, A.; Swartz, S.; et al. Estimates of the global, regional, and national morbidity, mortality, and aetiologies of lower respiratory tract infections in 195 countries: a systematic analysis for the Global Burden of Disease Study 2015. *Lancet Infect. Dis.* **2017**, *17*, 1133−1161.

(5) Su, F. Y.; Srinivasan, S.; Lee, B.; Chen, J.; Convertine, A. J.; West, T. E.; et al. Macrophage-targeted drugamers with enzyme-cleavable linkers deliver high intracellular drug dosing and sustained drug pharmacokinetics against alveolar pulmonary infections. *J. Controlled Release* **2018**, *287*, 1−11.

(6) Gupta, A.; Das, R.; Yesilbag Tonga, G.; Mizuhara, T.; Rotello, V. M. Charge-Switchable Nanozymes for Bioorthogonal Imaging of Biofilm-Associated Infections. *ACS Nano* **2018**, *12* (1), 89−94.

(7) Schillaci, D.; Spanò, V.; Parrino, B.; Carbone, A.; Montalbano, A.; Barraja, P.; et al. Pharmaceutical Approaches to Target Antibiotic Resistance Mechanisms. *J. Med. Chem.* **2017**, *60*, 8268−8297.

(8) Ghosh, C.; Sarkar, P.; Issa, R.; Haldar, J. Alternatives to Conventional Antibiotics in the Era of Antimicrobial Resistance. *Trends Microbiol.* **2019**, *27* (4), 323−338.

(9) Yılmaz, ć; Özcengiz, G. Antibiotics: Pharmacokinetics, toxicity, resistance and multidrug efflux pumps. *Biochem. Pharmacol.* **2017**, *133*, 43−62.

(10) Abed, N.; Couvreur, P. Nanocarriers for antibiotics: A promising solution to treat intracellular bacterial infections. *Int. J. Antimicrob. Agents* **2014**, *43*, 485−496.

(11) Flume, P. A.; VanDevanter, D. R. Clinical applications of pulmonary delivery of antibiotics. *Adv. Drug Delivery Rev.* **2015**, *85*, 1−6.

(12) Wang, Q.; Mi, G.; Hickey, D.; Li, Y.; Tu, J.; Webster, T. J.; et al. Azithromycin-loaded respirablemicroparticles for targeted pulmonary delivery for the treatment of pneumonia. *Biomaterials* **2018**, *160*, 107−123.
(13) Gupta, P. V.; Nirwane, A. M.; Belubbi, T.; Nagarsenker, M. S. Pulmonary delivery of synergistic combination of fluoroquinolone antibiotic complemented with proteolytic enzyme: A novel anti-microbial and antibiofilm strategy. *Nanomedicine* **2017**, *13*, 2371−2384.
(14) Xiong, M. H.; Bao, Y.; Yang, X. Z.; Zhu, Y. H.; Wang, J. Delivery of antibiotics with polymeric particles. *Adv. Drug Delivery Rev.* **2014**, *78*, 63−76.
(15) Rissler, J.; Gudmundsson, A.; Nicklasson, H.; Swietlicki, E.; Wollmer, P.; Löndahl, J. Deposition efficiency of inhaled particles (15−5000 nm) related to breathing pattern and lung function: an experimental study in healthy children and adults. *Part. Fibre Toxicol.* **2017**, *14* (1), 1−12.
(16) Chandel, A.; Goyal, A. K.; Ghosh, G.; Rath, G. Recent advances in aerosolised drug delivery. *Biomed. Pharmacother.* **2019**, *112*, 108601.
(17) Porsio, B.; Craparo, E. F.; Mauro, N.; Giammona, G.; Cavallaro, G. Mucus and cell-penetrating nanoparticles embedded in nano into micro formulations for pulmonary delivery of Ivacaftor in cystic fibrosis. *ACS Appl. Mater. Interfaces* **2018**, *10* (1), 165−181.
(18) Hidalgo, A.; Cruz, A.; Pérez-Gil, J. Barrier or carrier? Pulmonary surfactant and drug delivery. *Eur. J. Pharm. Biopharm.* **2015**, *95*, 117−127.
(19) Yang, Y.; Wu, Y.; Ren, Q.; Zhang, L. G.; Liu, S.; Zuo, Y. Y. Biophysical Assessment of Pulmonary Surfactant Predicts the Lung Toxicity of Nanomaterials. *Small Methods* **2018**, *2*, 1700367.
(20) Mousseau, F.; Le Borgne, R.; Seyrek, E.; Berret, J. F. Biophysicochemical Interaction of a Clinical Pulmonary Surfactant with Nanoalumina. *Langmuir* **2015**, *31*, 7346−7354.
(21) Nagao, M.; Fujiwara, Y.; Matsubara, T.; Hoshino, Y.; Sato, T.; Miura, Y. Design of Glycopolymers Carrying Sialyl Oligosaccharides for Controlling the Interaction with the Influenza Virus. *Biomacromolecules* **2017**, *18*, 4385−4392.
(22) Geng, J.; Mantovani, G.; Tao, L.; Nicolas, J.; Chen, G.; Wallis, R.; et al. Site-Directed Conjugation of "Clicked" Glycopolymers To Form Glycoprotein Mimics: Binding to Mammalian Lectin and Induction of Immunological Function. *J. Am. Chem. Soc.* **2007**, *129*, 15156−15163.
(23) Wang, Y.; Kotsuchibashi, Y.; Liu, Y.; Narain, R. Study of Bacterial Adhesion on Biomimetic Temperature Responsive Glycopolymer Surfaces. *ACS Appl. Mater. Interfaces* **2015**, *7*, 1652−1661.
(24) Lu, M.; Chen, F.; Cao, C.; Garvey, C. J.; Fletcher, N. L.; Houston, Z. H.; et al. Importance of Polymer Length in Fructose-Based Polymeric Micelles for an Enhanced Biological Activity. *Macromolecules* **2019**, *52*, 477−486.
(25) Lu, M.; Khine, Y. Y.; Chen, F.; Cao, C.; Garvey, C. J.; Lu, H.; et al. Sugar Concentration and Arrangement on the Surface of Glycopolymer Micelles Affect the Interaction with Cancer Cells. *Biomacromolecules* **2019**, *20*, 273−284.
(26) Portier, F.; Imberty, A.; Halila, S. Expeditious Synthesis of C-Glycosyl Barbiturate Ligands of Bacterial Lectins: From Monomer Design to Glycoclusters and Glycopolymers. *Bioconjugate Chem.* **2019**, *30*, 647−656.
(27) Pasparakis, G.; Cockayne, A.; Alexander, C. Control of Bacterial Aggregation by Thermoresponsive Glycopolymers. *J. Am. Chem. Soc.* **2007**, *129*, 11014−11015.
(28) Scolari, I. R.; Páez, P. L.; Sánchez-Borzone, M. E.; Granero, G. E. Promising Chitosan-Coated Alginate-Tween 80 Nanoparticles as Rifampicin Coadministered Ascorbic Acid Delivery Carrier Against Mycobacterium tuberculosis. *AAPS PharmSciTech* **2019**, *20* (67), 1−21.
(29) Scolari, I. R.; Páez, P. L.; Musri, M. M.; Petiti, J. P.; Torres, A.; Granero, G. E. Rifampicin loaded in alginate/chitosan nanoparticles as a promising pulmonary carrier against Staphylococcus aureus. *Drug Delivery Transl. Res.* **2020**, *10*, 1403−1417.
(30) Hohlfeld, J.; Fabel, H.; Hamm, H. The role of pulmonary surfactant in obstructive airways disease. *Eur. Respir. J.* **1997**, *10*, 482−491.
(31) Zuo, Y. Y.; Veldhuizen, R. A. W.; Neumann, A. W.; Petersen, N. O.; Possmayer, F. Current perspectives in pulmonary surfactant - Inhibition, enhancement and evaluation. *Biochim. Biophys. Acta, Biomembr.* **2008**, *1778*, 1947−1977.
(32) Autilio, C.; Pérez-Gil, J. Understanding the principle biophysics concepts of pulmonary surfactant in health and disease. *Arch Dis Child Fetal Neonatal* **2018**, *0*, F1−F9.
(33) Button, B.; Goodell, H. P.; Atieh, E.; Chen, Y.-C.; Williams, R.; Shenoy, S.; Lackey, E.; Shenkute, N. T.; Cai, L.-H.; Dennis, R. G.; Boucher, R. C.; Rubinstein, M.; et al. Roles of mucus adhesion and cohesion in cough clearance. *Proc. Natl. Acad. Sci. U. S. A.* **2018**, *115* (49), 12501−12506.
(34) Ostedgaard, L. S.; Moninger, T. O.; McMenimen, J. D.; Sawin, N. M.; Parker, C. P.; Thornell, I. M.; Powers, L. S.; Gansemer, N. D.; Bouzek, D. C.; Cook, D. P.; Meyerholz, D. K.; Abou Alaiwa, M. H.; Stoltz, D. A.; Welsh, M. J.; et al. Gel-forming mucins form distinct morphologic structures in airways. *Proc. Natl. Acad. Sci. U. S. A.* **2017**, *114* (26), 201703228.
(35) Hansen, I. M.; Ebbesen, M. F.; Kaspersen, L.; Thomsen, T.; Bienk, K.; Cai, Y.; et al. Howard. Hyaluronic Acid Molecular Weight-Dependent Modulation of Mucin Nanostructure for Potential Mucosal Therapeutic Applications. *Mol. Pharmaceutics* **2017**, *14*, 2359−2367.
(36) Coltart, D. M.; Royyuru, A. K.; Williams, L. J.; Glunz, P. W.; Sames, D.; Kuduk, S. D.; et al. Principles of Mucin Architecture: Structural Studies on Synthetic Glycopeptides Bearing Clustered Mono-, Di-, Tri-, and Hexasaccharide Glycodomains. *J. Am. Chem. Soc.* **2002**, *124*, 9833−9844.
(37) Kamaruzzaman, N. F.; Kendall, S.; Good, L. Targeting the hard to reach: challenges and novel strategies in the treatment of intracellular bacterial infections. *Br. J. Pharmacol.* **2017**, *174*, 2225−2236.
(38) Moreno-Sastre, M.; Pastor, M.; Salomon, C. J.; Esquisabel, A.; Pedraz, J. L. Pulmonary drug delivery: a review on nanocarriers for antibacterial chemotherapy. *J. Antimicrob. Chemother.* **2015**, *70*, 2945−2955.
(39) Prata, L. G.P. L.; Ovsyannikova, I. G.; Tchkonia, T.; Kirkland, J. L. Senescent cell clearance by the immune system: Emerging therapeutic opportunities. *Semin. Immunol.* **2018**, *40*, No. 101275.
(40) Gaines, G. L. *Insoluble monolayers at liquid-gas interfaces*; Interscience Publishers: New York, 1966.
(41) Yakubov, G. E.; Papagiannopoulos, A.; Rat, E.; Easton, R. L.; Waigh, T. A. Molecular Structure and Rheological Properties of Short-Side-Chain Heavily Glycosylated Porcine Stomach Mucin. *Biomacromolecules* **2007**, *8*, 3467−3477.
(42) Cohen, J. S.; Benton, A. S.; Nwachukwu, F.; Ozedirne, T.; Teach, S. J.; Freishtat, R. J. P-Glycoprotein Transporter Expression on A549 Respiratory Epithelial Cells Is Positively Correlated with Intracellular Dexamethasone Levels. *J. Invest. Med.* **2010**, *58* (8), 991−994.
(43) Murray, L. A.; Knight, D. A.; Laurent, G. J. Fibroblasts. Barnes, P. J., Drazen, J. M., Rennard, S. I., Thomson, N. C., Eds.; *Asthma and COPD: Basic Mechanisms and Clinical Management*, 2nd ed.; Elsevier, 2009; Chapter 15, pp 193−200.
(44) Koukourakis, M. I.; Kalamida, D.; Mitrakas, A. G.; Liousia, M.; Pouliliou, S.; Sivridis, E.; Giatromanolaki, A. Metabolic cooperation between co-cultured lung cancer cells and lung fibroblasts. *Lab. Invest.* **2017**, *97*, 1321−1331.
(45) International Standard Organization. In Biological Evaluation of Medical Devices Part 5: Tests for Cytotoxicity. In *Vitro Methods.*, 2009, pp 10993−10995.
(46) Bhunchu, S.; Rojsitthisak, P.; Rojsitthisak, P. Effects of preparation parameters on the characteristics of chitosan-alginate nanoparticles containing curcumin diethyl disuccinate. *J. Drug Delivery Sci. Technol.* **2015**, *28*, 64−72.

(47) Magnusson, P.; Dziendzikowska, K.; Oczkowski, M.Ł; Øvrevik, J.; Eide, D. M.; Brunborg, G.; Gutzkow, K. B.; Instanes, C.; Gajewska, M.; Wilczak, J.; Sapierzynski, R.Ł; Kamola, D.; Krolikowski, T.; Kruszewski, M.; Lankoff, A.; Mruk, R.; Duale, N.; Gromadzka-Ostrowska, J.; Myhre, O.; et al. Lung effects of 7- and 28-day inhalation exposure of rats to emissions from 1st and 2nd generation biodiesel fuels with and without particle filter - The Fuel Health project. *Environ. Toxicol. Pharmacol.* **2019**, *67*, 8−20.
(48) Haque, S.; Feeney, O.; Meeusen, E.; Boyd, B. J.; McIntosh, M. P.; Pouton, C. W.; Whittaker, M.; Kaminskas, L. M.; et al. Local inflammation alters the lung disposition of a drug loaded pegylated liposome after pulmonary dosing to rats. *J. Controlled Release* **2019**, *307*, 32−43.
(49) Schyns, J.; Bureau, F.; Marichal, T. Lung Interstitial Macrophages: Past, Present, and Future. *J. Immunol. Res.* **2018**, *2018*, 1−10.
(50) Schyns, J.; Bai, Q.; Ruscitti, C.; Radermecker, C.; De Schepper, S.; Chakarov, S.; Farnir, F.; Pirottin, D.; Ginhoux, F.; Boeckxstaens, G.; Bureau, F.; Marichal, T.; et al. Non-classical tissue monocytes and two functionally distinct populations of interstitial macrophages populate the mouse lung. *Nat. Commun.* **2019**, *10* (3964), 1−16.
(51) Coll-Bonfill, N.; Peinado, V. I.; Pisano, M. V.; Parrizas, M.; Blanco, I.; Evers, M.; Engelmann, J. C.; Garcia-Lucio, J.; Tura-Ceide, O.; Meister, G.; Barbera, J. A.; Musri, M. M.; et al. Slug Is Increased in Vascular Remodeling and Induces a Smooth Muscle Cell Proliferative Phenotype. *PLoS One* **2016**, *11* (7), e0159460.
(52) Beck-Broichsitter, M.; Bohr, A.; Ruge, C. A. Poloxamer-Decorated Polymer Nanoparticles for Lung Surfactant Compatibility. *Mol. Pharmaceutics* **2017**, *14* (10), 3464−3472.
(53) Knust, J.; Ochs, M.; Gundersen, H. J. G.; Nyengaard, J. R. Stereological Estimates of Alveolar Number and Size and Capillary Length and Surface Area in Mice Lungs. *Anat. Rec.* **2009**, *292*, 113−122.
(54) Schief, W. R.; Antia, M.; Discher, B. M.; Hall, S. B.; Vogel, V. Liquid-Crystalline Collapse of Pulmonary Surfactant Monolayers. *Biophys. J.* **2003**, *84* (6), 3792−3806.
(55) Zulueta Díaz Y de las, M.; Fanani, M. L. Crossregulation between the Insertion of Hexadecylphosphocholine (Miltefosine) into Lipid Membranes and Their Rheology and Lateral Structure. *Biochim. Biophys. Acta, Biomembr.* **2017**, *1859* (10), 1891−1899.
(56) Beck-Broichsitter, M.; Ruppert, C.; Schmehl, T.; Günther, A.; Seeger, W. Biophysical inhibition of synthetic vs. naturally-derived pulmonary surfactant preparations by polymeric nanoparticles. *Biochim. Biophys. Acta, Biomembr.* **2014**, *1838*, 474−481.
(57) Bansil, R.; Turner, B. S. The biology of mucus: Composition, synthesis and organization. *Adv. Drug Delivery Rev.* **2018**, *124*, 3−15.
(58) Ahmad, M.; Ritzoulis, C.; Chen, J. Shear and extensional rheological characterization of mucin solutions. *Colloids Surf., B* **2018**, *171*, 614−621.
(59) Hussell, T.; Bell, T. J. Alveolar macrophages: plasticity in a tissue-specific context. *Nat. Rev. Immunol.* **2014**, *14*, 81−93.
(60) Hu, G.; Christman, J. W. Editorial: Alveolar Macrophages in Lung Inflammation and Resolution. *Front. Immunol.* **2019**, *10*, 1−3.

https://dx.doi.org/10.1021/acs.molpharmaceut.0c00692
Mol. Pharmaceutics 2021, 18, 807−821